Response to RC1:

Authors: Xirui Ma, Yun Zhang, Panyan Ge, Yan Yin, Hepeng Zheng, Tingting Kang, Lingbing Bu, Wenjie Su, Donglin Yang, Qiangyue Xiang and Yinze Ran

We greatly appreciate your valuable time for reviewing our research paper and providing suggestions. ***(The blue text is in response to your comments, and the green text is for specific modifications in the paper. We also highlight revisions in the manuscript.)***

General Review:

This manuscript investigates an advection sea fog event over Qingbang Island in the East China Sea, with particular emphasis on the possible role of long-range transported dust aerosols. The study combines ground-based observations, Himawari-9 satellite products, and ERA5 reanalysis data to examine the evolution of aerosols, visibility, boundary-layer stability, radiation, turbulence, and synoptic conditions. The topic is scientifically interesting because sea fog under complex aerosol backgrounds remains insufficiently understood. The event classification into seven stages provides a relatively clear framework for organizing the life cycle of the dust–fog system, from dust passage to fog formation, mist maintenance, and dissipation. The attempt to link aerosol evolution, radiative forcing, boundary-layer stability, turbulence, and synoptic forcing into an integrated physical picture is potentially valuable for the sea-fog community.

However, I have substantial concerns regarding the strength of the evidence supporting several of the central conclusions. In its current form, the manuscript tends to overstate several causal mechanisms and requires a more rigorous treatment of uncertainty, observational limitations, and alternative explanations. In particular, the conclusions that dust aging enhanced hygroscopicity, that sulfate-coated dust replaced sea salt as the dominant CCN source, that dust radiative forcing produced the deep inversion layer, and that specific turbulence thresholds maintained sea fog are not sufficiently supported by the available observations. Many of these interpretations exceed the observational capability of the available dataset, remaining plausible hypotheses rather than demonstrated mechanisms. Stronger causal attribution would require additional evidence, quantitative analysis, or My major concerns are as follows:

Answer:

We sincerely appreciate the reviewer's valuable comments and suggestions. We have carefully revised the manuscript and figures in accordance with the specific recommendations provided.

Specific Review:

1. **The proposed dust-aging mechanism lacks direct observational evidence.**

The main logical chain linking transported dust aerosols to sea fog evolution remains largely hypothetical. The observations show elevated dust aerosol loading before fog formation and increased

sulfate aerosol contribution during the fog period, but there is no direct evidence demonstrating that these sulfate aerosols originated from aged dust particles coated by sulfate. In fact, during the fog period, the satellite product indicates relatively low dust contribution but high sulfate contribution. If the aerosols were truly dominated by sulfate-coated dust particles, the manuscript should explain why the identified dust fraction becomes so low during fog formation. This raises an important question regarding either the interpretation of the aging process or the reliability and physical meaning of the satellite-derived aerosol component classification under foggy conditions.

Answer: We sincerely thank the reviewer for the meticulous evaluation of the strength of the dust-aging argument in our study. The reviewer's comments are highly constructive and have led to major revisions of the original manuscript.

In the original manuscript, the discussions on dust aging were scattered across the analyses of Figs. 4, 5, 6, and 7. While each section presented specific observational features and relevant citations, the mutual independence of these diverse observational aspects, and the overarching speculative storyline they collectively form, were not clearly articulated. This fragmented presentation could indeed easily give the reviewer the impression that excessive argumentative weight was assigned to individual observational aspects. Furthermore, the original manuscript contained overly assertive expressions, such as "confirmed", "was mainly attributed to", "indicates ··· efficient CCN", and "explosive hygroscopic growth", which exceed what the observations of this study can directly support.

Prompted by the reviewer's comments, a careful re-examination also revealed an inaccuracy in our physical interpretation. The original manuscript interpreted the particle-size modal shift observed in the dry-state PM measurements as "explosive hygroscopic growth". However, because our PM measurement system employs a heated inlet for dehumidification, particle-bound water is removed before the sample air enters the optical sensor. Therefore, the modal shift observed in the dry-state measurements cannot be directly attributed to hygroscopic growth from a physical perspective.

We fully accept the reviewer's criticisms regarding all the issues mentioned above and have made systematic revisions in the revised manuscript.

Regarding the Usage of Satellite Data:

At the end of Section 2.2 (Lines 144–146) in the original manuscript, we stated that the satellite aerosol composition data during the sea fog period (Stages 4–6) were used merely as a qualitative reference, while the quantitative analysis mainly focused on Stages 1–3 and Stage 7. However, quantitative expressions such as "contributed the most to sea fog" appeared in the analysis of Fig. 5 in the original manuscript, contradicting this statement. We sincerely apologize for this oversight. We have removed such expressions in the revised manuscript and replaced them with qualitative descriptions. The argumentation for dust aging relies strictly on satellite data from the quantitatively usable stages (Stages 1–3 and Stage 7) and does not depend on data from the fog period. We have strengthened the explanation of this stage-by-stage data processing in Section 2.2 of the revised manuscript and reiterated it in the analysis of Fig. 5 (Section 3.2) for clarity.

The explanation added to the Fig. 5 analysis section (Line 285 of the original manuscript) regarding satellite data usage is as follows:

To further study the impact of aerosols on the formation and dissipation mechanism of this sea fog, based on the aerosol component AOD product of the H-9 satellite, the bilinear interpolation method was used. The temporal variation characteristics of AOD for sulfate, black carbon, organic carbon, sea salt, and dust aerosols at Qingbang Island in the East China Sea were calculated (Fig. 5(a)). Based on this, the average contribution rates of different types of aerosols during the entire study period were calculated (Fig. 5(b)). In this study, satellite derived aerosol composition data are utilized as quantitative observations during Stages 1–3 and 7, whereas they are limited to qualitative reference during the fog period (Stages 4–6).

Key Clarification Regarding PM Measurements:

The PM mass concentration measurement equipment used in this study performs sampling by heating the drawn in air and reducing its relative humidity to below 40%. Specifically, ambient air is drawn in by a sampling pump at a constant flow rate, and before entering the optical measurement chamber, its relative humidity is reduced to below 40% through a heating tube, ensuring the particles are in a dry state during measurement. The measured PM_1, $PM_{2.5}$, and PM_{10} correspond to the dry aerosol mass, effectively eliminating the direct interference from liquid fog droplets and the moisture of hydrated particles.

The text at Line 123 of the original manuscript has been revised to:

Due to the lack of conventional meteorological data with high spatiotemporal resolution in this sea area, raw observation data with a temporal resolution of 10 s were obtained by the automatic weather station (AWS) independently established in this study. The main observation parameters include air temperature (T), relative humidity (RH), pressure (Pa), wind speed (WS), wind direction (WD), particulate matter mass concentration (PM_1、$PM_{2.5}$、PM_{10}), and visibility (Vis). To eliminate high-frequency random noise and ensure data stability, all surface meteorological elements were subjected to strict quality control and were averaged into time series data with 1 min intervals for subsequent analysis. The PM mass concentration measurement equipment used in this study performs sampling by heating the drawn in air and reducing its relative humidity to below 40%. Specifically, ambient air is drawn in by a sampling pump at a constant flow rate, and before entering the optical measurement chamber, its relative humidity is reduced to below 40% through a heating tube, ensuring the particles are in a dry state during measurement. The measured PM_1, $PM_{2.5}$, and PM_{10} correspond to the dry aerosol mass, effectively eliminating the direct interference from liquid fog droplets and the moisture of hydrated particles.

Regarding the hardware limitations of this study：

We must candidly acknowledge that this study did not have direct-observation single-particle chemical analysis and mixing-state characterization instruments (Scanning electron microscopy (SEM), Transmission electron microscopy (TEM) and Nanoscale secondary ion mass spectrometry (NanoSIMS)) that could directly demonstrate that the sulfate aerosol originated from aged dust particles coated with sulfate. For an island-type observation station such as Qingbang Island, deploying such large laboratory-grade single-particle aerosol instruments faces substantial practical challenges in terms of site space and equipment logistics. This is an objective methodological limitation of this study.

Drawing on the following five mutually independent observational aspects, together with the available literature on Asian dust aging, this study proposes a reasonable speculation:

(1) Fig. 4 shows that the dust was transported from Inner Mongolia through Shaanxi, Shanxi, and Shanghai to Qingbang Island in the East China Sea, passing through regions with elevated SO_2, NO_x, and NH_3 emissions. During long-range transport, dust readily reacts chemically with SO_2 and NO_x, which favours dust aging and sulfate formation. The chemical environment is consistent with the conditions required for heterogeneous sulfate formation on dust surfaces.

(2) Quantitatively usable stages in Fig. 5: During the early periods of Stages 1–3 (before 06:00 on the 25th), dust and sulfate coexisted spatio-temporally, which was conducive to their mixing and chemical reactions. In the late period of Stage 3 (after 06:00 on the 25th, approximately 10.8 hours prior to fog formation), the sulfate AOD increased while the dust component AOD decreased. This scenario aligns well with existing literature reporting that dust aging and the Fe-S coupling mechanism accelerate sulfate formation (Zhuang et al., 1992; Duce et al., 1980; Martin et al., 1994).

(3) Fig. 6(a) shows that during the dust passage period in Stage 2, the proportions of aerosol particles in the 0-1 μm and 1-2.5 μm size ranges increased significantly, with the aerosols mainly concentrated in the 0-2.5 μm range. As the dust transport passed through regions with strong pollution emissions, the dust particles may have mixed and interacted with regional pollutants and undergone some degree of chemical aging.

(4) Figs. 6(a, b) show that from late Stage 3 to early Stage 4, the modal shift reflected the evolution of dry aerosol particles rather than the direct effect of liquid water. This is consistent with the physical process in which aerosols, after undergoing heterogeneous reactions (e.g., sulfate coating onto dust surfaces) and aqueous-phase processing under near-saturated conditions in the atmosphere. Simultaneously, the MEE increased significantly by 2.3 times, reaching 125 m^2/g. This indicates that the extinction efficiency of aerosols in a wet state has significantly improved, which is consistent with the phenomenon that aerosols undergo hygroscopic growth in a high-humidity environment. These two independent observations jointly support that aerosols have undergone chemical and physical evolution in the atmosphere from different physical perspectives.

(5) Fig. 7 shows that sea fog can be triggered at low PM_1, $PM_{2.5}$, and PM_{10} mass concentrations, indicating that the aerosols possess relatively strong hygroscopicity.

Based on these five observational results, together with the literature on long-range transported dust particles (Li et al., 2025; Tobo et al., 2010; Sullivan et al., 2009; Ma et al., 2013; Yin et al., 2007) in which sulfate and nitrate coatings on the surfaces of dust particles have been directly observed as the literature reference. This study proposes the reasonable speculation that the transported dust may have undergone aging, with some particles becoming coated by sulfate to form internally mixed aerosols with a dust-core and sulfate-shell structure that exhibits strong hygroscopicity. This is a reasonable speculation based on the combination of multiple observational results and the literature, rather than a microphysical mechanism directly verified in this study. Direct verification at the aerosol particle level necessitates concurrent single particle chemical and mixing state measurements during similar events in the future. This will be the primary direction of our future research.

Specific Revisions to the Manuscript:

A new paragraph (synthesizing the 5 observational points, literature deduction, and explicit uncertainty statement) has been added after Section 3.2 (in the original manuscript):

The results of Fig. 7 (a, b, c) all show that there was a typical exponential decay relationship between visibility and aerosol mass concentration. However, the decay rate was strictly controlled by the RH. During the low RH phase of dust passage (as shown in the blue-purple colour results at around 2-5 km in the figure), the sensitivity of visibility to PM concentration was relatively low. The exponential decay result showed a high exponential decay rate in the sea fog under high RH conditions. When the visibility was in the range of 0-1 km, the mass concentrations of PM_1, $PM_{2.5}$, and PM_{10} were in the ranges of 26-77, 38-157, and 47-275 μgm^{-3}, respectively. The low critical thresholds for sea fog occurrence were 26, 38, and 47 μgm^{-3}, respectively. This significant result indicates that only a low aerosol mass concentration is needed to trigger sea fog. This suggests that the aerosols are highly hygroscopic.

Combining the results of Figs. 4–7: (1) Fig. 4 shows that the dust was transported from Inner Mongolia through Shaanxi, Shanxi, and Shanghai to Qingbang Island in the East China Sea, passing through regions with elevated SO_2, NO_x, and NH_3 emissions. During long-range transport, dust readily reacts chemically with SO_2 and NO_x, which favours dust aging and sulfate formation. The chemical environment is consistent with the conditions required for heterogeneous sulfate formation on dust surfaces. (2) Quantitatively usable stages in Fig. 5: During the early periods of Stages 1–3 (before 06:00 on the 25th), dust and sulfate coexisted spatio-temporally, which was conducive to their mixing and chemical reactions. In the late period of Stage 3 (after 06:00 on the 25th, approximately 10.8 hours prior to fog formation), the sulfate AOD increased while the dust component AOD decreased. This scenario aligns well with existing literature reporting that dust aging and the Fe-S coupling mechanism accelerate sulfate formation (Zhuang et al., 1992; Duce et al., 1980; Martin et al., 1994). (3) Fig. 6(a) shows that during the dust passage period in Stage 2, the proportions of aerosol particles in the 0-1 μm and 1-2.5 μm size ranges increased significantly, with the aerosols mainly concentrated in the 0-2.5 μm range. As the dust transport passed through regions with strong pollution emissions, the dust particles may have mixed and interacted with regional pollutants and undergone some degree of chemical aging. (4) Figs. 6(a, b) show that from late Stage 3 to early Stage 4, the modal shift reflected the evolution of dry aerosol particles rather than the direct effect of liquid water. This is consistent with the physical process in which aerosols, after undergoing

heterogeneous reactions (e.g., sulfate coating onto dust surfaces) and aqueous-phase processing under near-saturated conditions in the atmosphere. Simultaneously, the MEE increased significantly by 2.3 times, reaching 125 m^2/g. This indicates that the extinction efficiency of aerosols in a wet state has significantly improved, which is consistent with the phenomenon that aerosols undergo hygroscopic growth in a high-humidity environment. These two independent observations jointly support that aerosols have undergone chemical and physical evolution in the atmosphere from different physical perspectives. (5) Fig. 7 shows that sea fog can be triggered at low PM_1, PM2.5, and PM_{10} mass concentrations, indicating that the aerosols possess relatively strong hygroscopicity. This is a reasonable speculation based on the combination of multiple observational results and the literature, rather than a microphysical mechanism directly verified in this study. Based on these five observational results, together with the literature on long-range transported dust particles (Li et al., 2025; Tobo et al., 2010; Sullivan et al., 2009; Ma et al., 2013; Yin et al., 2007) in which sulfate and nitrate coatings on the surfaces of dust particles have been directly observed as the literature reference. This study proposes the reasonable speculation that the transported dust may have undergone aging, with some particles becoming coated by sulfate to form internally mixed aerosols with a dust-core and sulfate-shell structure that exhibits strong hygroscopicity. This study did not have direct-observation single-particle chemical analysis and mixing-state characterization instruments (Scanning electron microscopy (SEM), Transmission electron microscopy (TEM) and Nanoscale secondary ion mass spectrometry (NanoSIMS)). These could directly demonstrate that the sulfate aerosol originated from aged dust particles coated with sulfate. For an island-type observation station such as Qingbang Island, deploying such large laboratory grade single particle aerosol instruments faces substantial practical challenges in terms of site space and equipment logistics. Direct verification at the aerosol particle level necessitates concurrent single particle chemical and mixing state measurements during similar events in the future. This will be the primary direction of our future research.

Regarding the content on dust aging, overly strong expressions in the original manuscript such as "confirmed", "was mainly attributed to", and "indicates ... efficient CCN" have been consistently adjusted to more cautious wording. The main revisions are as follows:

The Abstract has been revised to:

Evolution mechanisms of explosive advection sea fog coupled with long-range dust transport over East Asia remain unclear. This study investigates a dust–advection sea fog event using ground-based observations, Himawari-9 satellite products, and ERA5 reanalysis data. Results show that dust may have undergone aging during transport, promoting sea fog under high humidity (RH > 90%). Before sea fog formation (Stage 3: 12:40-16:47 on the 25th) and during the sea fog period (Stage 4: 16:47-19:30 on the 25th), the proportion of 0-1 μm particles decreased by 18% and 24%, respectively. The proportion of 1-2.5 μm particles increased by 5% and 4%, respectively. The proportion of 2.5-10 μm particles increased by 13% and 20%, respectively. This phenomenon is consistent with aerosols undergoing heterogeneous reactions and aqueous-phase processes, which may be associated with dust aging. Unlike classical advection cooling, radiative forcing of dust and cold air formed a deep inversion (9°C) before fog, which with warm-moist advection suppressed turbulent mixing and provided a favourable thermodynamic background for fog maintenance. The threshold ranges of turbulence parameters (U, TKE, u_*, I_u, I_v, I_w, u_*) were relatively distinct when sea fog maintains visibility within 1 km. The system showed a significant characteristic of turbulence acting first and fog responding later during the late stage of mist. The downward longwave radiation (DLR) was highly sensitive to changes in fog layer structure. Fog dissipation was caused by circulation adjustment and re-invasion of dry-cold dust carried by northerly winds, destroying phase equilibrium. These findings advance understanding of sea fog under complex aerosol backgrounds.

The relevant content of the Fig. 5 analysis (lines 289–317 of the original manuscript) has been revised. The revised version is as follows:

From Fig. 5 (a) and (b), it can be seen that dust aerosol particles dominated and contributed the most during Stage 1-3(06:00 on March 25) before the outbreak of sea fog. The aerosol contributions from high to low were dust, sulfate, organic carbon, black carbon, and sea salt aerosols. It is notable that the contribution of sea salt aerosols was the lowest. This

indicates that the aerosols at the observation site were mainly dominated by long-distance dust transport during this stage. This indicates that the aerosols at the observation site were mainly dominated by long-distance dust transport during this stage. During this stage, dust and sulfate coexisted spatially and temporally, which was conducive to their mixing and chemical reactions.

During the pre-formation phase of advection sea fog (Stage 3, 06:00-16:47 on the 25th), the dust AOD was gradually decreasing. The sulfate AOD was gradually increasing and became the dominant component. The contribution of sea salt remained at a low level. Previous studies have shown that in the marine atmospheric environment, Fe ions on the surface of dust can accelerate the formation of sulfate through the Fe-S coupling mechanism (Zhuang et al., 1992; Duce et al., 1980; Martin et al., 1994). This is highly consistent with the gradually increasing trend of sulfate AOD observed in our study. Previous studies have shown that dust particles can form a mixed structure of dust core and sulfate shell during the aging process. This internal mixing state can enhance the hygroscopicity of dust and effectively reduce the critical supersaturation required for its activation. This makes it easier to transform into cloud condensation nuclei (CCN) (Li et al., 2025; Tobo et al., 2010; Sullivan et al., 2009; Ma et al., 2013; Yin et al., 2007). Such a scenario may have occurred during the event. In addition, the large accumulation of sulfate aerosols can cause a cooling effect on the atmosphere due to its negative forcing on solar radiation. Combined with the continuous moist advection, this further promotes the formation of sea fog.

During the sea fog and maintenance stages (Stage 4-6), the sulfate AOD remained at a high level. This is consistent with the research results of Zhao (Zhao et al., 2022). However, these results are intended strictly as a qualitative reference rather than for quantitative identification. During the mist dissipation phase (Stage 7), the dust AOD increased significantly. This may cause cooling through the combined effect of scattering to reduce surface shortwave radiation and cold air. At the same time, it changed the stratification stability. This finally led to the evaporation of fog droplets, the increase of visibility, and the dissipation of mist. This further verifies the conjecture in Fig. 4 (e) and (f) that the dissipation of sea fog is related to the second passage of dust. In summary, dust aerosols may have played a dual role in this dust-sea fog event. During the pre-formation phase of sea fog (Stage 3) and the mist dissipation phase (Stage 7), the temperatures both showed a decreasing trend. In Stage 3, when the RH increased, dust may have transformed into more hygroscopic mixed-state aerosols through the aging process, promoting the formation of sea fog. In Stage 7, when the RH decreased, dust inhibited the maintenance of mist.

The relevant content of the Fig. 6 analysis (lines 338–341 of the original manuscript) has been revised. The revised version is as follows:

In the early period of Stage 3, aerosols were mainly submicron particles (0-1 μm). However, after the RH increased to 90% at 12:40 on March 25, a significant modal shift occurred in the aerosol particle size distribution. During Stage 3 (12:40-16:47 on March 25) and the early period of Stage 4 (16:47-19:30 on March 25), the proportion of particles with sizes of 0-1 μm decreased by 18% and 24%, respectively, while the proportion of particles with sizes of 1-2.5 μm increased by 5% and 4%, respectively, and the proportion of particles with sizes of 2.5-10 μm increased by 13% and 20%, respectively. This modal shift reflects the actual variation in the dry aerosol mass distribution. This is consistent with aerosols undergoing heterogeneous reactions (e.g., sulfate coating on dust surfaces) and aqueous-phase processing in the atmosphere. In the middle and late period of Stage 4, the proportions of particles with sizes of 0-1 μm and 1-2.5 μm showed oscillating increases, while the proportion of particles with sizes of 2.5-10 μm showed an overall oscillating decrease. This phenomenon was attributed to the gravitational settling and wet removal effect of large fog droplets. During Stage 5, the proportions of all particle sizes showed oscillating variation trends, and the PM mass concentrations showed an overall oscillating decrease. This indicates the dynamic competition between external transport and wet removal by fog droplets, ultimately resulting in the wet removal effect of fog on aerosols.

The relevant content of the Fig. 7 analysis (lines 372–389 of the original manuscript) has been revised. The revised version is as follows:

To understand how aerosol mass concentration and RH affect the macroscopic visibility evolution of this event, the meteorological station observation data (PM mass concentration, Vis, RH) during the entire process were used. This aimed to explore the relationship of visibility to PM mass concentration and its sensitivity to RH (Fig. 7).

The results of Fig. 7 (a, b, c) all show that there was a typical exponential decay relationship between visibility and aerosol mass concentration. However, the decay rate was strictly controlled by the RH. During the low RH phase of dust passage (as shown in the blue-purple colour results at around 2-5 km in the figure), the sensitivity of visibility to PM concentration was relatively low. The exponential decay result showed a high exponential decay rate in the sea fog under high RH conditions. When the visibility was in the range of 0-1 km, the mass concentrations of PM_1, $PM_{2.5}$, and PM_{10} were in the ranges of 26-77, 38-157, and 47-275 μgm^{-3}, respectively. The low critical thresholds for sea fog occurrence were 26, 38, and 47 μgm^{-3}, respectively. This significant result indicates that only a low aerosol mass concentration is needed to trigger sea fog. This suggests that the aerosols are highly hygroscopic.

The relevant content of the Section 4 Conclusions (lines 577–589 of the original manuscript) has been revised. The revised version is as follows:

This event indicates that long-distance transported dust aerosols have a promoting effect on sea fog formation under high RH conditions. Dust aerosols originating from Mongolia passed through the observation site under the guidance of the westerly jet, causing the near-surface PM_{10} mass concentration to explosively increase to 469 μgm^{-3}. Different from the traditional view in sea fog research that sea salt aerosols act as CCN, this study found that during the Stage 3 to early Stage 4, dust and sulfate aerosols showed high coupling in time and space (sulfate AOD showed an increasing trend). During Stage 3 (12:40-16:47 on March 25) and early Stage 4 (16:47-19:30 on March 25), the aerosol particle size distribution showed obvious modal shift. The proportion of 0-1 μm particles decreased by 18% and 24%, respectively, while the proportion of 1-2.5 μm particles increased by 5% and 4%, respectively, and the proportion of 2.5-10 μm particles increased by 13% and 20%, respectively. This modal shift reflects the actual variation in the dry aerosol mass distribution. This is consistent with aerosols undergoing heterogeneous reactions (e.g., sulfate coating on dust surfaces) and aqueous-phase processing in the atmosphere. This also confirms that the cross-modal transformation of aerosols to fog droplets is the core microphysical cause of the sharp drop of Vis to below 1.0 km. The fact that aerosols with a low PM mass concentration threshold can trigger sea fog formation implies their strong hygroscopicity. Based on the independent observations above, and drawing analogies from existing literature on the aging of cross-sea dust, a reasonable speculation is that the long-range transported dust may have undergone aging over the ocean. Some dust particles might be coated by sulfate to form a "dust core–sulfate shell" aerosol structure, exhibiting strong hygroscopicity. Consequently, sulfate aerosols may act as one of the crucial CCN sources during this sea fog event. While this hypothesis has not yet been directly verified, it will serve as the primary focus of our future research.

2. **The attribution of inversion formation to dust radiative forcing is not sufficiently supported.**

The manuscript interprets changes in the relative fractions of 0–1, 1–2.5, and 2.5–10 μm particles as evidence for hygroscopic growth and activation into fog droplets. However, during fog events, PM measurements can be strongly contaminated by hydrated aerosols and fog droplets depending on the inlet configuration, drying conditions, sampling efficiency, and sensor response characteristics. Consequently, the apparent increase in coarse-mode mass may simply reflect direct sampling of fog droplets or highly hydrated particles rather than a true aerosol-size modal shift. Without demonstrating that fog droplets did not contaminate the PM measurements, the interpretation of aerosol hygroscopic growth and size evolution should be substantially moderated.

Answer: We thank the reviewer for the comments and suggestions on the physical rigor of the attribution between dust radiative forcing and the inversion. We have carefully considered the reviewer's suggestions and have made detailed revisions to the relevant content.

Revisions to the Abstract:

Evolution mechanisms of explosive advection sea fog coupled with long-range dust transport over East Asia remain unclear. This study investigates a dust–advection sea fog event using ground-based observations, Himawari-9 satellite products, and

ERA5 reanalysis data. Results show that dust may have undergone aging during transport, promoting sea fog under high humidity (RH>90%). Before sea fog formation (Stage 3: 12:40-16:47 on the 25th) and during the sea fog period (Stage 4: 16:47-19:30 on the 25th), the proportion of 0-1 μm particles decreased by 18% and 24%, respectively. The proportion of 1-2.5 μm particles increased by 5% and 4%, respectively. The proportion of 2.5-10 μm particles increased by 13% and 20%, respectively. This phenomenon is consistent with aerosols undergoing heterogeneous reactions and aqueous-phase processes, which may be associated with dust aging. Before fog formation, the cold air advection and radiative forcing of dust co-acted to deepen a 9°C inversion, which with warm-moist advection suppressed turbulent mixing and provided a favourable thermodynamic background for fog maintenance. The threshold ranges of turbulence parameters (U, TKE, u_*, I_u, I_v, I_w, u_*) were relatively distinct when sea fog maintains visibility within 1 km. The system showed a significant characteristic of turbulence acting first and fog responding later during the late stage of mist. The downward longwave radiation (DLR) was highly sensitive to changes in fog layer structure. Fog dissipation was caused by circulation adjustment and re-invasion of dry-cold dust carried by northerly winds, destroying phase equilibrium. These findings advance understanding of sea fog under complex aerosol backgrounds.

The relevant content of Section 3.3 (lines 401–413 and 431–435 of the original manuscript) has been revised. The revised version is as follows:

Fig. 8 shows that from Stage 1 to Stage 2, the radiation field evolved from the typical clear-sky diurnal characteristics to one accompanied by aerosol radiative effects. During Stage 2, the solar diurnal cycle together with the co-acting effects of cold-air advection and dust jointly modulated the attenuation of DSR at the surface. DLR did not weaken with the decrease of solar elevation angle, in the early period of dust passage, but remained at about 335 $W \cdot m^{-2}$. This observation is consistent with the influence of the dust layer on the surface longwave budget through thermal radiation after shortwave absorption. However, with sunset and the gravitational settling of dust, ULR showed an attenuation trend. Rn turned negative early at 17:30 on March 24, indicating that the surface energy budget reversed from surplus to deficit. In Stage 3, with the increase of sulfate aerosol concentration and its mixing with dust, aerosols showed strong scattering characteristics. Observations showed that DSR decreased by 744 $W \cdot m^{-2}$ from 12:30 to 17:00 on March 25. The decrease rate was 8% higher than that under clear-sky background (the same period in Stage 1-2). This further reflects that the radiative properties of different types of aerosols can change the surface-atmosphere radiation balance and heating or cooling rate, and then change the PBL structure. The strong scattering effect of sulfate aerosols combined with water vapor accumulation provided the necessary thermodynamic preconditions for the subsequent condensation and outbreak of sea fog in the near-surface layer.

Fig. 9 shows that an inversion structure began to form in the near-surface layer at 10:00 on March 24, mainly concentrated at 0.4-1 km. Its occurrence and development were accompanied by both the synoptic-scale cold-air advection at low levels ((Fig. 12(d-1)) and the continuous increase of dust AOD observed by satellite on March 24 (Fig. 5a). With the continuous passage and settling of the dust carried by the cold air, the near-surface inversion progressively strengthened. The maximum inversion reached 9 °C, and the thickness of the inversion layer also expanded significantly. This strong inversion layer was favourable for the accumulation of dust aerosols of sea surface and provided initial thermal conditions for the stabilization of the lower atmosphere. From 09:00 to 16:47 on March 25, with the establishment of sea breeze carrying warm and moist airflow over the cold sea surface, a continuously stable and deeper inversion layer formed in the boundary layer.

The relevant content of Section 4 Conclusions (lines 590–601 of the original manuscript) has been revised. The revised version is as follows:

The cold-air intrusion and dust radiative forcing co-acted to change the boundary-layer thermodynamic structure, constructing a favourable background for the formation of advection sea fog. During Stage 2, the solar diurnal cycle together with the co-acting effects of cold-air advection and dust jointly modulated the attenuation of DSR at the surface. This caused the near-surface temperature to drop sharply by 5.0°C within 5 hours, forming an inversion. The inversion was mainly concentrated at 0.4-1 km, with the maximum inversion intensity reaching 9°C. Previous studies on advection sea fog mostly emphasized the advective cooling effect. However, this study found that under a high-dust background, dust

radiative effects combined with synoptic-scale cold-air advection to deepen the inversion during the early stage of Stage 2. This process enhanced the stability of the boundary layer in advance. This early inversion (Stage 2) superimposed with the subsequently established warm and moist advection (the SAT-SST was 1.8°C in Stage 3), providing favourable thermodynamic conditions and stratification stability for the occurrence of sea fog. During the advection sea fog period (Stage 4), the dense fog layer caused the net radiation (Rn) to remain continuously negative. This kept the MEE at a high level of 70-120 m^2/g, establishing the long-term maintenance of the sea fog system. The study found that DLR was the most sensitive to the state changes of sea fog (fluctuations of fog top height, uneven liquid water content, and fog layer thickness).

3. **Interpretation of PM-derived particle-size evolution is problematic during fog conditions.**

The manuscript interprets changes in the relative fractions of 0–1, 1–2.5, and 2.5–10 μm particles as evidence for hygroscopic growth and activation into fog droplets. However, during fog events, PM measurements can be strongly contaminated by hydrated aerosols and fog droplets depending on the inlet configuration, drying conditions, sampling efficiency, and sensor response characteristics. Consequently, the apparent increase in coarse-mode mass may simply reflect direct sampling of fog droplets or highly hydrated particles rather than a true aerosol-size modal shift. Without demonstrating that fog droplets did not contaminate the PM measurements, the interpretation of aerosol hygroscopic growth and size evolution should be substantially moderated.

Answer: We sincerely thank the reviewer for this valuable comment. The misunderstanding indeed arose from our insufficient description of the instrument. We have added a description of the operating principle of the PM mass concentration measurement instrument in Section 2.1 (lines 118–123 of the original manuscript). The added content reads as follows:

Due to the lack of conventional meteorological data with high spatiotemporal resolution in this sea area, raw observation data with a temporal resolution of 10 s were obtained by the automatic weather station (AWS) independently established in this study. The main observation parameters include air temperature (T), relative humidity (RH), pressure (Pa), wind speed (WS), wind direction (WD), particulate matter mass concentration (PM_1、$PM_{2.5}$、PM_{10}), and visibility (Vis). To eliminate high-frequency random noise and ensure data stability, all surface meteorological elements were subjected to strict quality control and were averaged into time series data with 1 min intervals for subsequent analysis. The PM mass concentration measurement equipment used in this study performs sampling by heating the drawn-in air and reducing its relative humidity to below 40%. Specifically, ambient air is drawn in by a sampling pump at a constant flow rate, and before entering the optical measurement chamber, its relative humidity is reduced to below 40% through a heating tube, ensuring the particles are in a dry state during measurement. The measured PM_1, $PM_{2.5}$, and PM_{10} correspond to the dry aerosol mass, effectively eliminating the direct interference from liquid fog droplets and the moisture of hydrated particles.

4. **The interpretation of Figure 11 overstates turbulence "threshold" behavior and sensitivity.**

The manuscript interprets the relatively narrow ranges of turbulence-related variables under low-visibility conditions as evidence of strong fog sensitivity to these variables. However, the narrower ranges observed during fog periods may simply reflect the limited meteorological conditions sampled during the relatively short fog duration. The analysis does not exclude the possibility that fog can exist outside these parameter ranges, or does it establish causality or sensitivity. Therefore, the mechanistic interpretation substantially exceeds what the observations can support.

Answer: We sincerely thank the reviewer for the valuable suggestions and comments. The reviewer is entirely correct that the narrower range may merely reflect the limited meteorological conditions sampled within the

relatively short fog period. We have removed the inappropriate over-interpretation. The revisions are as follows:

The Abstract has been revised to:

Evolution mechanisms of explosive advection sea fog coupled with long-range dust transport over East Asia remain unclear. This study investigates a dust-advection sea fog event using multi-source data. Results show that dust may have undergone aging during transport, promoting sea fog under high humidity (RH>90%). Before sea fog formation (Stage 3: 12:40-16:47 on the 25th) and during the sea fog period (Stage 4: 16:47-19:30 on the 25th), the proportion of 0-1 μm particles decreased by 18% and 24%, respectively. The proportion of 1-2.5 μm particles increased by 5% and 4%, respectively. The proportion of 2.5-10 μm particles increased by 13% and 20%, respectively. This phenomenon is consistent with aerosols undergoing heterogeneous reactions and aqueous-phase processes, which may be associated with dust aging. Before fog formation, the cold air advection and radiative forcing of dust co-acted to deepen a 9°C inversion, which with warm-moist advection suppressed turbulent mixing and provided a favourable thermodynamic background for fog maintenance. The threshold ranges of turbulence parameters (U, TKE, u_*, I_u, I_v, I_w, u_*) were relatively distinct when sea fog maintains visibility within 1 km. The system showed a significant characteristic of turbulence acting first and fog responding later during the late stage of mist. The downward longwave radiation (DLR) was highly sensitive to changes in fog layer structure. Fog dissipation was caused by circulation adjustment and re-invasion of dry-cold dust carried by northerly winds, destroying phase equilibrium. These findings advance understanding of sea fog under complex aerosol backgrounds.

The relevant content of the Fig. 11 analysis (lines 507–508 of the original manuscript) has been revised. The revised version is as follows:

A clear result in Fig. 11 (a-f) all consistently show, when PM_{10} mass concentration exceeded 80 μgm^{-3}, Vis was mostly below 1 km. Based on this characteristic threshold, the threshold ranges of turbulence parameters for maintaining sea fog below 1 km were also relatively obvious. The thresholds of U and TKE were concentrated in the ranges of 3.1-5.1 ms^{-1} and 1.91-2.74 m^2s^{-2}, respectively. It is notable that the u_* was limited to a significantly narrow range of 0.62-0.69 ms^{-1}. The thresholds of I_u, I_v, and I_w were concentrated in 0.2-0.4, 0.8-0.95, and 0.21-0.31, respectively. This moderate turbulence threshold range established a quasi-steady dynamic equilibrium. This turbulence intensity was sufficient to maintain the co-suspension of high-concentration aerosols and fog droplets under near-saturated conditions. At the same time, it was effectively limited below the critical value, thus avoiding the dissipation of sea fog caused by stronger entrainment or mechanical turbulence at higher intensity.

Some English language polishing is also needed throughout the manuscript. Several sentences are awkward or difficult to follow. Examples include lines 56–62, 75–77, 92 ("law" is not an appropriate word to describe aerosol/fog evolution), 118–119, and 570–571.

Answer: We thank the reviewer for the comments. The wording at the locations mentioned by the reviewer was indeed problematic. We have revised each of these in turn. The revisions are as follows:

Lines 56–62 have been revised to:

Studies have shown that dust from northern China and Mongolia can be transported over long distances across the Yellow Sea, East Sea, and even to the Pacific Ocean (Cahill et al., 2003; Sullivan et al., 2007). While traditional views consider pure dust to be hydrophobic and inhibitory to fog formation (Li et al., 2025), dust particles can undergo significant atmospheric aging during transport. Through coagulation, cloud processing, and heterogeneous surface reactions, dust can mix with anthropogenic pollutants (e.g., ammonium sulfate, ammonium nitrate, biomass burning particles) (Li et al., 2025; Clarke et al., 2004; Korhonen et al., 2003; Yin et al., 2002; Zhang and Iwasaka, 2004; Zhang et al., 2003) as well as marine biogenic dimethyl sulfide (DMS) (Zhuang et al., 1992; Zhang et al., 2000). These complexes mixing substantially enhance the hygroscopicity of long-range transported dust (Li et al., 2025; Tobo et al., 2010; Sullivan et al., 2009; Ma et al., 2013;

Yin et al., 2007). Due to the very complex interactions of multiple influencing factors between long-range transported dust and sea fog, the details of the effects of long-range transported dust on sea fog processes have not been well understood.

Lines 75–77 have been revised to:

The role in marine advection fog remains unclear. In fact, radiation is a key factor regulating the life cycle of sea fog (Fernando et al., 2021; Yun and Ha, 2022). Furthermore, observational and simulation studies have demonstrated that turbulence significantly influences the macrophysics of fog (Ye and Zhang, 2015; Porson et al., 2011), such as modulating the fog top height (Zhou and Ferrier, 2008). However, moderate turbulence can promote fog development (Zhou and Ferrier, 2008; Price, 2019).

At line 92, "laws" has been revised to "characteristics":

The aim of this study is to clarify the comprehensive driving mechanism of sea fog formation and dissipation in the dust aerosol environment by exploring the evolution characteristics of aerosol microphysics, radiation and boundary layer thermodynamic structure, turbulent dynamic characteristics, as well as synoptic conditions and air-sea conditions during this event.

Lines 118–119 have been revised to:

To address the scarcity of high-spatiotemporal-resolution meteorological data in this marine region, we deployed an automatic weather station (AWS) to collect raw observational data at a 10-second temporal resolution. The main observation parameters include air temperature (T), relative humidity (RH), pressure (Pa), wind speed (WS), wind direction (WD), particulate matter mass concentration (PM_1、$PM_{2.5}$、PM_{10}), and visibility (Vis).

Lines 570–571 have been revised to:

Using Himawari-9 satellite remote sensing data, high-resolution ground-based observations at Qingbang Island in the East China Sea, and ERA5 reanalysis data, we conducted a detailed full-life-cycle study of a dust–advection sea fog event during 24–28 March 2025. Through comprehensive analysis of aerosol microphysical properties, radiation and boundary layer thermodynamic structure, turbulence dynamic characteristics, and the evolution of synoptic situation and air-sea conditions, the key parameters during this process were quantified. The comprehensive mechanism of typical dust-advection sea fog event was systematically studied (Fig. 13). The main conclusions are as follows:

Additional specific comments:

Line 15: “multi-source” data should be described more specifically (e.g., ground-based observations, satellite products, and reanalysis data).

Answer: We sincerely thank the reviewer for pointing out that the expression "multi-source data" in the Abstract of the original manuscript is overly general. Following the reviewer's suggestion, it has been revised to:

Evolution mechanisms of explosive advection sea fog coupled with long-range dust transport over East Asia remain unclear. This study investigates a dust–advection sea fog event using ground-based observations, Himawari-9 satellite products, and ERA5 reanalysis data. Results show that dust may have undergone aging during transport, promoting sea fog under high humidity (RH>90%). Before sea fog formation (Stage 3: 12:40-16:47 on the 25th) and during the sea fog period (Stage 4: 16:47-19:30 on the 25th), the proportion of 0-1 μm particles decreased by 18% and 24%, respectively. The proportion of 1-2.5 μm particles increased by 5% and 4%, respectively. The proportion of 2.5-10 μm particles increased by 13% and 20%, respectively. This phenomenon is consistent with aerosols undergoing heterogeneous reactions and aqueous-phase processes, which may be associated with dust aging. Before fog formation, the cold air advection and radiative forcing of dust co-acted to deepen a 9°C inversion, which with warm-moist advection suppressed turbulent mixing and provided a

favourable thermodynamic background for fog maintenance. The threshold ranges of turbulence parameters (U, TKE, u_*, I_u, I_v, I_w, u_*) were relatively distinct when sea fog maintains visibility within 1 km. The system showed a significant characteristic of turbulence acting first and fog responding later during the late stage of mist. The downward longwave radiation (DLR) was highly sensitive to changes in fog layer structure. Fog dissipation was caused by circulation adjustment and re-invasion of dry-cold dust carried by northerly winds, destroying phase equilibrium. These findings advance understanding of sea fog under complex aerosol backgrounds.

Line 24: A narrow range of u* does not necessarily imply high sensitivity.

Answer: We thank the reviewer for the detailed suggestions. Following the reviewer's suggestions, the relevant content has been revised as follows:

Evolution mechanisms of explosive advection sea fog coupled with long-range dust transport over East Asia remain unclear. This study investigates a dust–advection sea fog event using ground-based observations, Himawari-9 satellite products, and ERA5 reanalysis data. Results show that dust may have undergone aging during transport, promoting sea fog under high humidity (RH>90%). Before sea fog formation (Stage 3: 12:40-16:47 on the 25th) and during the sea fog period (Stage 4: 16:47-19:30 on the 25th), the proportion of 0-1 μm particles decreased by 18% and 24%, respectively. The proportion of 1-2.5 μm particles increased by 5% and 4%, respectively. The proportion of 2.5-10 μm particles increased by 13% and 20%, respectively. This phenomenon is consistent with aerosols undergoing heterogeneous reactions and aqueous-phase processes, which may be associated with dust aging. Before fog formation, the cold air advection and radiative forcing of dust co-acted to deepen a 9°C inversion, which with warm-moist advection suppressed turbulent mixing and provided a favourable thermodynamic background for fog maintenance. The threshold ranges of turbulence parameters (U, TKE, u_*, I_u, I_v, I_w, u_*) were relatively distinct when sea fog maintains visibility within 1 km. The system showed a significant characteristic of turbulence acting first and fog responding later during the late stage of mist. The downward longwave radiation (DLR) was highly sensitive to changes in fog layer structure. Fog dissipation was caused by circulation adjustment and re-invasion of dry-cold dust carried by northerly winds, destroying phase equilibrium. These findings advance understanding of sea fog under complex aerosol backgrounds.
A clear result in Fig. 11 (a-f) all consistently show, when PM_{10} mass concentration exceeded 80 μgm^{-3}, Vis was mostly below 1 km. Based on this characteristic threshold, the threshold ranges of turbulence parameters for maintaining sea fog below 1 km were also relatively obvious. The thresholds of U and TKE were concentrated in the ranges of 3.1-5.1 ms^{-1} and 1.91-2.74 m^2s^{-2}, respectively. It is notable that the u_* was limited to a significantly narrow range of 0.62-0.69 ms^{-1}. The thresholds of I_u, I_v, and I_w were concentrated in 0.2-0.4, 0.8-0.95, and 0.21-0.31, respectively. This moderate turbulence threshold range established a quasi-steady dynamic equilibrium. This turbulence intensity was sufficient to maintain the co-suspension of high-concentration aerosols and fog droplets under near-saturated conditions. At the same time, it was effectively limited below the critical value, thus avoiding the dissipation of sea fog caused by stronger entrainment or mechanical turbulence at higher intensity.

Line 68: "warm-moist air flows over cold sea surfaces" is not advective cooling, it is warm advection.

Answer: We sincerely thank the reviewer for pointing this out. We agree that the physical movement of "warm-moist air flowing over cold sea surfaces" is precisely defined as "warm advection".

Our original intention was to highlight the "advection cooling mechanism" which is the characteristic formation mechanism specific to sea fog. Specifically, during this warm advection process (where air temperature is higher than sea surface temperature), the sensible heat exchange from the air to the sea surface becomes dominant, causing the advected warm-moist air to cool and condense into fog.

To be meteorologically rigorous, we have revised the sentence to clearly articulate the causal relationship: it is the warm advection process that drives the sensible heat loss, ultimately constituting the advection cooling mechanism.

Line 68 has been revised to:

The strong scattering and absorption of shortwave radiation by dust aerosols can cause significant cooling of near-surface atmosphere (Obiso et al., 2024; Wang et al., 2024). For advection sea fog, the classical theory mainly emphasizes the advection cooling mechanism, in which warm advection (warm-moist air flowing over cold sea surfaces) drives sensible heat loss, causing the air to cool and condense (Yang et al., 2024).

Figure 1: Better indicate the nested spatial relationship among the panels. It would also help to expand panel (c) to better show the surrounding marine and continental environment and the distance from the mainland.

Answer: We thank the reviewer for this valuable suggestion, which significantly improves the geographical context of our study area. We have redrawn Figure 1 accordingly.

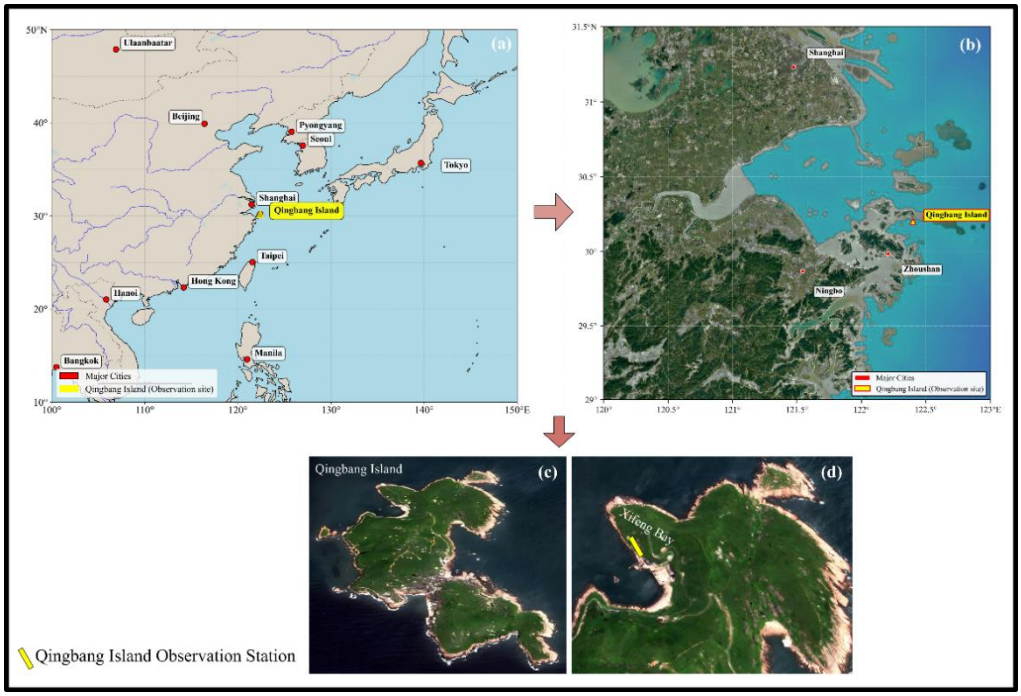

Lines 100 and 112: There are two Section 2.1 headings.

Answer: We sincerely thank the reviewer for the careful reading. Two consecutive "Section 2.1" headings did indeed appear in the original manuscript, and we apologize for this oversight. In the revised manuscript, the heading at the original line 112 has been corrected to "2.2 Instruments and data analysis", and the subsequent "2.3" section number has been adjusted accordingly to ensure the continuity and correctness of the section numbering. The specific changes are as follows:

2.2 Instruments and data analysis

2.3 Methods

Line 113: Revise to "The data used in this study include:" since "mainly" implies additional datasets not described.

Answer: We thank the reviewer for the suggestion. This has been revised exactly as the reviewer requested. The modification is as follows:

The data used in this study include: (1) surface meteorological observation data; (2) radiation data; (3) near-surface turbulence observation data; (4) microwave radiometer retrieval data; (5) Himawari-9 satellite data(https://www.eorc.jaxa.jp/ptree/index.html); (6) ERA5 reanalysis data(https://cds.climate.copernicus.eu/). The data sources and instrument descriptions are shown in Table 1.

Line 123: Please specify what quality-control procedures were applied.

Answer: First, we sincerely thank the reviewer for this excellent suggestion. According to your advice, the modification is as follows:

To address the scarcity of high-spatiotemporal-resolution meteorological data in this marine region, we deployed an automatic weather station (AWS) to collect raw observational data at a 10-second temporal resolution. The main observation parameters include air temperature (T), relative humidity (RH), pressure (Pa), wind speed (WS), wind direction (WD), particulate matter mass concentration (PM_1、$PM_{2.5}$、PM_{10}), and visibility (Vis). To eliminate high-frequency random noise and ensure data stability, all surface meteorological elements were subjected to strict quality control. The specific procedures included: (1) physical limit checks to remove physically impossible values (e.g., relative humidity > 100% or < 0%, or negative wind speeds); (2) spike detection to eliminate isolated high-frequency noise and sudden unrealistic jumps; and (3) constant value checks to remove invalid data caused by temporary sensor malfunctions. Finally, the processed data were averaged into time series with 1-min intervals for subsequent analysis. The PM mass concentration measurement equipment used in this study performs sampling by heating the drawn-in air and reducing its relative humidity to below 40%. Specifically, ambient air is drawn in by a sampling pump at a constant flow rate, and before entering the optical measurement chamber, its relative humidity is reduced to below 40% through a heating tube, ensuring the particles are in a dry state during measurement. The measured PM_1, $PM_{2.5}$, and PM_{10} correspond to the dry aerosol mass, effectively eliminating the direct interference from liquid fog droplets and the moisture of hydrated particles.

Line 129: What retrieval algorithm was used for the microwave radiometer temperature profiles? Please discuss retrieval uncertainty and potential limitations. The sharp temperature transitions in Fig. 9 (especially on 03-28) may require additional discussion regarding retrieval reliability.

Answer: We sincerely appreciate the reviewer's professional and insightful question regarding the microwave radiometer (MWR) data. The content in line 129 of the text has also been elaborately supplemented.

(1). Retrieval Algorithm: The vertical temperature profiles were retrieved using a Neural Network (NN) algorithm based on the radiation brightness temperatures of oxygen molecules. To ensure optimal regional accuracy and reliability, this NN algorithm was specifically trained using a comprehensive historical dataset comprising 10 years of local balloon-borne radiosonde data.

(2). Reliability of the Sharp Transitions in Fig. 9 (March 28): We have carefully re-examined the sharp temperature transitions observed on March 28 (Stage 7). We confirm that this transition is physically real and atmospheric-driven, rather than an artifact of the retrieval algorithm. This period corresponds to the fog dissipation phase, during which a strong, dry-cold continental air mass driven by accelerated northerly winds (8 – 10m/s) rapidly invaded the observation site (as shown in the synoptic analysis in Fig. 12(a-3, c-3)). This intense synoptic forced cooling was synchronously and independently recorded by our surface automatic weather station (AWS), thereby cross-validating the reliability of the sharp thermal transition captured by the MWR.

(3). The content on line 129 of the original manuscript has been revised as follows:

Radiation parameters were measured by a four-component radiometer (CNR4). This instrument can simultaneously measure downward shortwave radiation (DSR), upward shortwave radiation (USR), downward longwave radiation (DLR), and upward longwave radiation (ULR). Net radiation (Rn) was calculated based on the surface radiation balance equation: Rn = (DSR - USR) + (DLR - ULR). To match the analysis scale of boundary layer fluxes, all radiation component data were processed into 30-min averages. In addition, a ground-based microwave radiometer (RPG-HATPRO) was used. Vertical profiles of air temperature in the boundary layer with high temporal resolution were obtained through retrieval algorithms. Vertical profiles of air temperature in the boundary layer were retrieved using a Neural Network (NN) algorithm based on the observed radiation brightness temperatures of oxygen molecules. To ensure optimal regional accuracy and

representativeness, the NN algorithm was systematically trained using a localized dataset comprising 10 years of historical balloon-borne radiosonde observations.

Line 137: Please clarify what is meant by "commonly used steps in fog detection."

Answer: We sincerely thank the reviewer for this valuable suggestion. We apologize for the confusion, which was likely caused by our unclear presentation in the original manuscript.

For fog area identification from the Himawari-9 satellite data, we adopted the brightness-temperature-difference (BTD) method, which is a widely used standard technique for nighttime fog and low-cloud detection (Kim et al., 2019). The BTD was computed as BTD=BT3.89-BT11.24, where BT3.89 and BT11.24 are the brightness temperatures at the mid-infrared (3.89 μm) and thermal infrared (11.24 μm) channels, respectively. For daytime periods, true-colour composites were utilized primarily for visual confirmation of the sea fog distribution.

The content on line 129 of the original manuscript has been revised as follows:

For large-scale monitoring, L1 data from Himawari-9 (H-9), the new-generation geostationary meteorological satellite of the Japan Meteorological Agency (JMA), was used in this study. The satellite is equipped with the Advanced Himawari Imager (AHI), which has the capability of high-frequency and multi-spectral observations (Bessho et al., 2016). For fog area identification from the Himawari-9 satellite data, we adopted the brightness-temperature-difference (BTD) method, which is a widely used standard technique for nighttime fog and low-cloud detection (Kim et al., 2019). The BTD was computed as BTD=BT3.89-BT11.24, where BT3.89 and BT11.24 are the brightness temperatures at the mid-infrared (3.89 μm) and thermal infrared (11.24 μm) channels, respectively. For daytime periods, true-colour composites were utilized primarily for visual confirmation of the sea fog distribution. For aerosol optical depth (AOD) data, the AHI L3 gridded aerosol product provided by JAXA Himawari Monitor (supported by the MASINGAR model system) was used. This product constrains the Meteorological Research Institute (MRI) aerosol transport model by assimilating AOD retrieved from H-9. Hourly AOD for components including sulfate, organic carbon, black carbon, sea salt, and dust can be output. During sea fog occurrences, satellite retrievals may be filtered out or contaminated by cloud screening mechanisms. In this case, model outputs lack direct observational constraints. Therefore, during sea fog occurrences, this AOD data was mainly used as a qualitative or semi-quantitative reference for the regional background aerosol environment. It was not used as an accurate observational basis for aerosol microphysical changes within the fog.

Figure 2 and several later figures: The plotted region is too large. A more focused regional domain would improve readability.

Answer: We highly appreciate the reviewer's constructive suggestion, which indeed helps to improve the readability and focus of the figures. We have reduced the drawing area for Figures 2 and 4 in the original manuscript. However, for Figure 12, we have retained the original drawing range of the figure. The formation of this advection sea fog and the long-range transport of dust aerosols are deeply driven by synoptic-scale circulation patterns (e.g., the Mongolian cyclone and westerly jet). Keeping a broader regional domain in Figure 12 is physically essential to fully illustrate the macro-scale atmospheric forcing, the origins of the air masses, and the complete transport pathways of the dust from inland to the ocean. We kindly ask the reviewer to appreciate that, due to the synoptic-scale nature of the analysis, the larger plotting domain of Figure 12 is retained. The revised results are as follows:

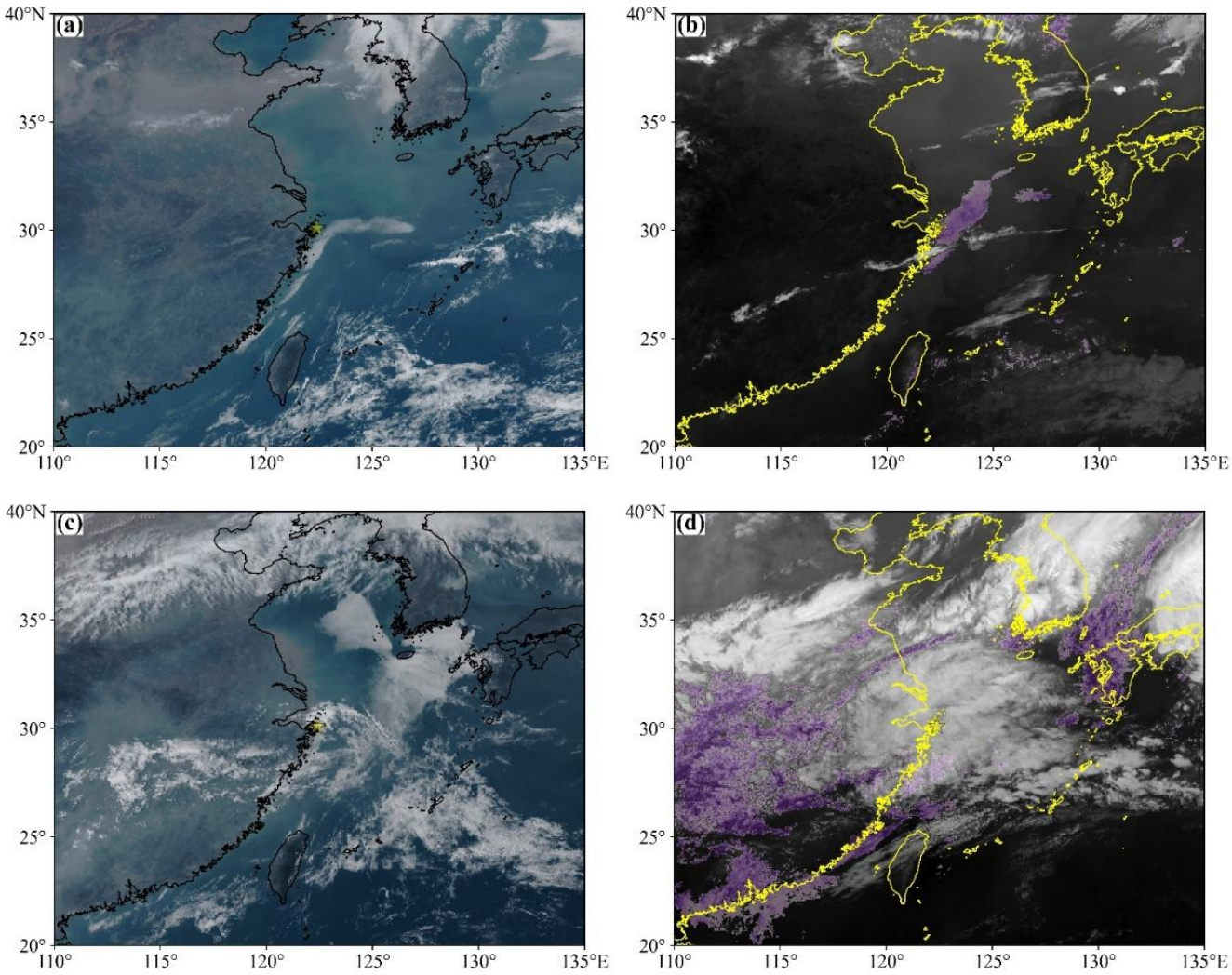

Figure 2: Sea fog monitoring images from the H-9 satellite. (a, c are the AHI RGB true-colour images at 09:00 LST on March 25 and 15:00 LST on March 26, respectively (local standard time (LST) = Universal Time Coordinated (UTC) + 8 h). b, d are the sea fog identification images at 18:00 LST on March 25 and 00:00 LST on March 28, respectively. Purple indicates fog identified at nighttime. The yellow pentagram indicates the observation site.)

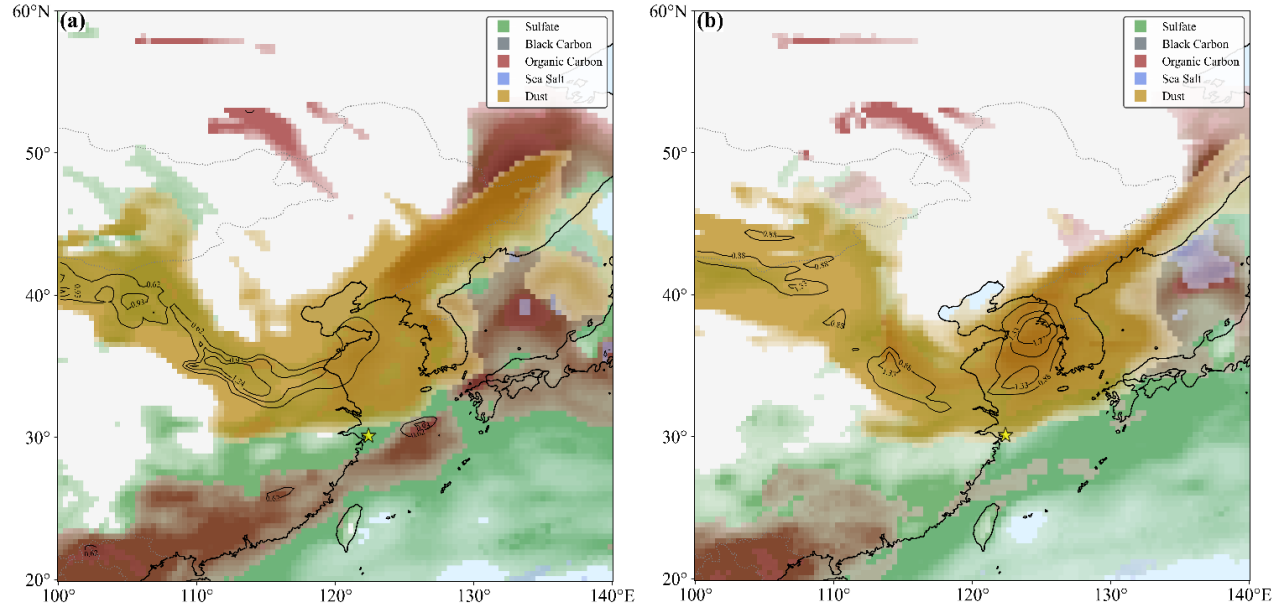

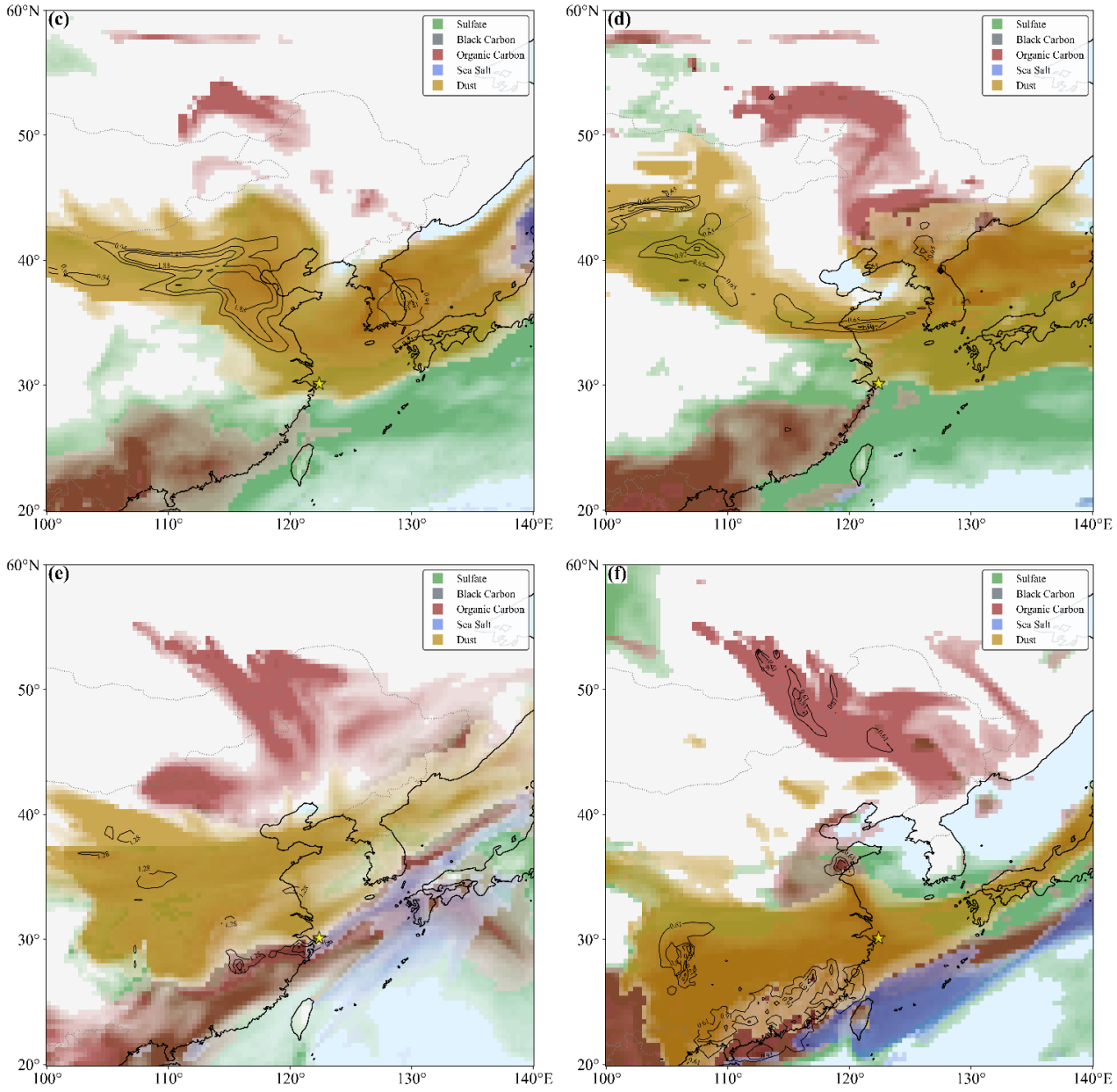

Figure 4: (a), (b), (c), (d), (e), and (f) show the distribution of different types of aerosols at 08:00 LST on March 24 (Stage 1: Pre-dust phase), 15:00 LST on March 24 (Stage 2: Dust phase), 00:00 LST on March 25, 15:00 LST on March 25 (Stage 3: Pre-formation phase of advection sea fog), 18:00 LST on March 27, and 18:00 LST on March 28 (Stage 7: Dissipation phase of mist), respectively. In the figure, green, gray, red, blue, and yellow represent sulfate, black carbon, organic carbon, sea salt, and dust aerosols, respectively.

Lines 215–217: Is the increase in aerosol mass concentration alone sufficient to identify the aerosols as dust? Any other direct evidence supporting this?

Answer: We sincerely appreciate the reviewer's rigorous and insightful question. We fully agree that an isolated explosive increase in PM mass concentrations is insufficient to uniquely identify the aerosols as dust.

To address this, we have comprehensively revised the description of Stage 2 in the manuscript. Instead of relying solely on PM concentrations, we have integrated a composite surface meteorological signature. These surface observation features, in conjunction with the satellite data and circulation analysis presented in the subsequent sections, jointly support the identification of this stage as the dust passage period. We have revised the relevant content from page 215 to 217 in the original manuscript. The revised results are as follows:

Stage 2 was affected by strong external disturbance. The PM mass concentrations showed explosive increases during this period. The peak values of PM_1, $PM_{2.5}$, and PM_{10} at 17:08 on March 24 were 267, 460, and 469 μg/m³, respectively (an increase of 11-14 times). This trend is consistent with the explosive input characteristics of dust aerosols (Rodríguez et al., 2024). During this stage, the average visibility was 2.4 km and the relative humidity remained at a low level of 40-65% (Table 2); at the PM peak, the visibility dropped sharply by 28.4% to 1.79 km, showing a strict inverse trend with PM mass concentration changes. The PM mass concentration peak (17:08) was synchronous with the wind speed peak (6.3 m/s). In addition, the event occurred during a concurrent cold-air intrusion in late March, within the dust season. These strongly coupled surface features are similar to those of long-range dust transport. Therefore, in conjunction with the satellite data and circulation analysis evidence presented in subsequent sections (Sections 3.2 and 3.5), this stage is identified as the dust passage period. The cold-air intrusion combined with the dust radiative effects intensified the near-surface temperature drop (a decrease of 5.0°C within 5 hours, with a cooling rate of about 1.0°C/h). In addition, the pressure showed an increase during 16:27-20:00. This may be related to the thermodynamic pressurization effect of aerosol increase on the local boundary layer (Luo et al., 2022).

Figure 5: Why are sea salt aerosols so few at a marine site? Is this physically reasonable or potentially related to retrieval uncertainty? Please also clarify how the satellite aerosol composition product is derived. If the satellite product is treated as reliable, how is the high-sulfate/low-dust condition connected with the proposed dust-aging mechanism?

Answer: We sincerely thank the reviewer for these insightful questions regarding Figure 5.

(1) Regarding the low sea salt aerosols: The low sea-salt contribution during Stages 1–3 is physically reasonable and correctly reflects the synoptic situation. Although Qingbang Island is a marine site, this specific event was dominated by long-range-transported continental aerosols and dust driven by the Mongolian cyclone and strong northwesterly winds. Together with the effect of particle deposition, the sea-salt AOD remained persistently low. During the sea-fog period, wet deposition by fog droplets also continuously removed sea-salt particles. A similar phenomenon of "low sea-salt contribution in coastal sea-fog conditions" has also been reported by Zhao et al. (2022) in their Arctic sea-fog study.

(2) Regarding the derivation of the satellite aerosol composition product: We would like to clarify that the AHI L3 aerosol component AOD product from JAXA Himawari Monitor used in this study is a hybrid product based on the MASINGAR (Model of Aerosol Species IN the Global AtmospheRe) chemistry transport model of MRI/JMA combined with assimilation of the total AOD retrieved from the Himawari satellite. Specifically, the total AOD comes from satellite retrieval, while the partitioning into the five components (sulfate, black carbon, organic carbon, sea salt, dust) is provided by the model and adjusted through total-AOD assimilation. A brief description of this data source was given in the original Section 2.2, and further details have been added in the revised manuscript.

(3) How is the high-sulfate / low-dust condition during the fog period connected with the proposed dust-aging mechanism: We would like to emphasize that the dust-aging argument in this study does not rely on the satellite component-AOD state during the fog period (Stages 4–6). Rather, it is based on the satellite data during Stage 2 and the later part of Stage 3, combined with the analysis of the near-surface data and existing literature on the aging of long-range-transported dust, to make a reasonable speculation. This point has been addressed in detail in our response to Comment 1.

We have revised the content related to the source of AOD data in Section 2.2 of the original manuscript. The revised results are as follows:

For aerosol optical depth (AOD) data, the AHI L3 gridded aerosol product provided by JAXA Himawari Monitor (supported by the MASINGAR model system) was used. This product constrains the Meteorological Research Institute (MRI) aerosol transport model by assimilating AOD retrieved from H-9. Hourly AOD for components including sulfate, organic carbon, black carbon, sea salt, and dust can be output. Specifically, only the total AOD is retrieved from H-9. The

partitioning into the individual aerosol components is provided by the MASINGAR model and adjusted through the total AOD assimilation. During sea fog occurrences, satellite retrievals may be filtered out or contaminated by cloud screening mechanisms. In this case, model outputs lack direct observational constraints. Therefore, during sea fog occurrences, this AOD data was mainly used as a qualitative or semi-quantitative reference for the regional background aerosol environment. It was not used as an accurate observational basis for aerosol microphysical changes within the fog.

Figure 5b: A bar plot or stacked-fraction plot would be more appropriate than a contour plot for showing aerosol component contributions.

Answer: We sincerely thank the reviewer for this excellent suggestion on data visualization. Following your valuable advice, we have replotted Figure 5(b) as a stacked-fraction plot (or stacked bar chart). This new visualization more accurately and intuitively illustrates the temporal evolution of the percentage contribution of each aerosol component, summing to 100% at any given time step. The revised results of Figure 5(b) in the original manuscript are as follows:

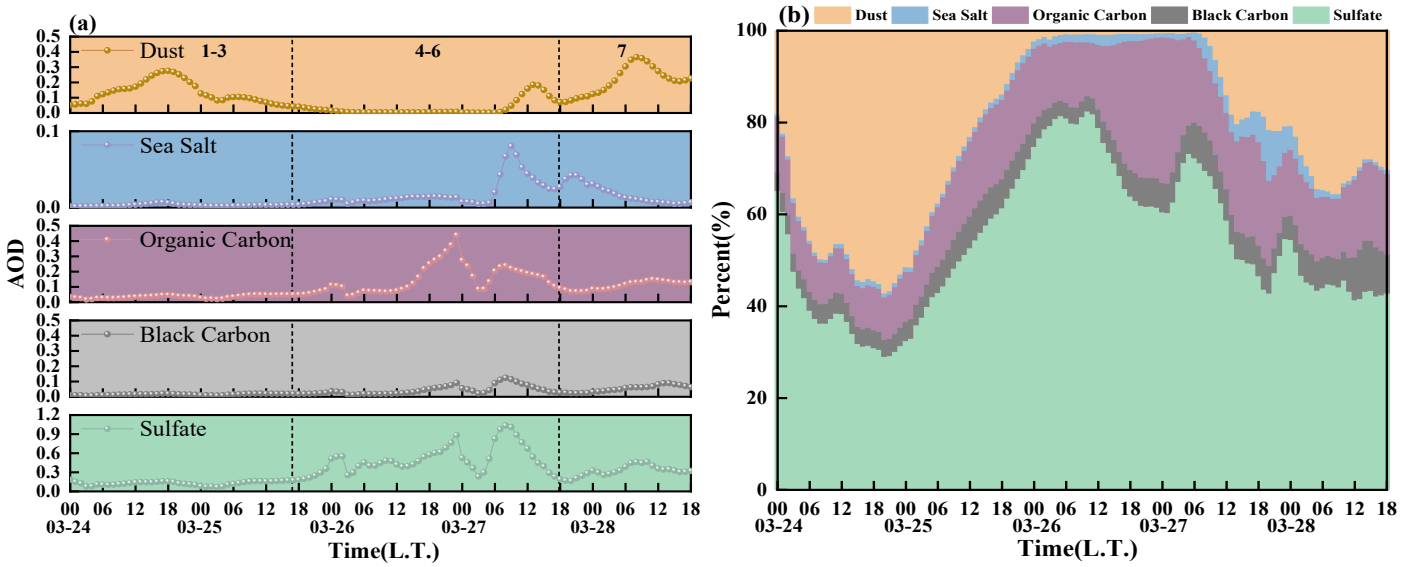

Figure 5: (a) and (b) show the temporal variation of AOD and the contribution rates of sulfate, black carbon, organic carbon, sea salt, and dust aerosols at Qingbang Island in the East China Sea, respectively.

Line 586: How can changes in bulk aerosol size distribution be directly linked to hygroscopicity changes of an individual aerosol component?

Answer: We sincerely thank the reviewer for the question. We completely agree that changes in the bulk aerosol size distribution (such as the mass ratios of PM_1, PM2.5, and PM_{10}) cannot be directly linked to the hygroscopicity changes of an individual aerosol component. The original statement "This significantly enhanced the hygroscopicity of dust" indeed overreached in the level of inference.

In our revision in response to Comment 1 and 3, the corresponding statement has been adjusted to:

Due to the lack of conventional meteorological data with high spatiotemporal resolution in this sea area, raw observation data with a temporal resolution of 10 s were obtained by the automatic weather station (AWS) independently established in this study. The main observation parameters include air temperature (T), relative humidity (RH), pressure (Pa), wind speed (WS), wind direction (WD), particulate matter mass concentration (PM_1、$PM_{2.5}$、PM_{10}), and visibility (Vis). To eliminate high-frequency random noise and ensure data stability, all surface meteorological elements were subjected to strict quality control and were averaged into time series data with 1 min intervals for subsequent analysis. The PM mass concentration measurement equipment used in this study performs sampling by heating the drawn-in air and reducing its relative humidity to below 40%. Specifically, ambient air is drawn in by a sampling pump at a constant flow

rate, and before entering the optical measurement chamber, its relative humidity is reduced to below 40% through a heating tube, ensuring the particles are in a dry state during measurement. The measured PM_1, $PM_{2.5}$, and PM_{10} correspond to the dry aerosol mass, effectively eliminating the direct interference from liquid fog droplets and the moisture of hydrated particles.

In the early period of Stage 3, aerosols were mainly submicron particles (0-1 μm). However, after the RH increased to 90% at 12:40 on March 25, a significant modal shift occurred in the aerosol particle size distribution. During Stage 3 (12:40-16:47 on March 25) and the early period of Stage 4 (16:47-19:30 on March 25), the proportion of particles with sizes of 0-1 μm decreased by 18% and 24%, respectively, while the proportion of particles with sizes of 1-2.5 μm increased by 5% and 4%, respectively, and the proportion of particles with sizes of 2.5-10 μm increased by 13% and 20%, respectively. This modal shift reflects the actual variation in the dry aerosol mass distribution. This is consistent with aerosols undergoing heterogeneous reactions (e.g., sulfate coating on dust surfaces) and aqueous-phase processing in the atmosphere. In the middle and late period of Stage 4, the proportions of particles with sizes of 0-1 μm and 1-2.5 μm showed oscillating increases, while the proportion of particles with sizes of 2.5-10 μm showed an overall oscillating decrease. This phenomenon was attributed to the gravitational settling and wet removal effect of large fog droplets. During Stage 5, the proportions of all particle sizes showed oscillating variation trends, and the PM mass concentrations showed an overall oscillating decrease. This indicates the dynamic competition between external transport and wet removal by fog droplets, ultimately resulting in the wet removal effect of fog on aerosols.

Lines 590–594: The attribution of thermodynamic structure changes to dust radiative effects remains insufficiently demonstrated. A decrease in DSR represents reduced heating rather than direct atmospheric cooling. Please clarify how this mechanism could produce cooling rates approaching 1 K/hr.

Answer: We thank the reviewer for raising this critical physical point. The reviewer is entirely correct that a decrease in DSR represents reduced shortwave heating rather than direct atmospheric cooling; a DSR decrease alone cannot account for a near-surface cooling rate on the order of 1 K/h.

The DSR attenuation during Stage 2 is not the result of dust radiative effects alone, but rather an observable manifestation of the joint modulation by three factors — the solar diurnal cycle, cold-air advection, and dust radiative effects. Likewise, the near-surface temperature drop of 5°C/5h (≈1.0°C/h) during Stage 2 is the joint result of these three factors, not a causal product of DSR attenuation itself.

In response to this comment, the corresponding paragraphs in Section 3.3 (Fig. 8 analysis) and in the conclusions section of the original manuscript have been revised. The revisions are as follows:

Section 3.3 (Fig. 8 analysis) has been revised to:

Fig. 8 shows that from Stage 1 to Stage 2, the radiation field evolved from the typical clear-sky diurnal characteristics to one accompanied by aerosol radiative effects. During Stage 2, the solar diurnal cycle together with the co-acting effects of cold-air advection and dust jointly modulated the attenuation of DSR at the surface. DLR did not weaken with the decrease of solar elevation angle, in the early period of dust passage, but remained at about 335 $W \cdot m^{-2}$. This observation is consistent with the influence of the dust layer on the surface longwave budget through thermal radiation after shortwave absorption. However, with sunset and the gravitational settling of dust, ULR showed an attenuation trend. Rn turned negative early at 17:30 on March 24, indicating that the surface energy budget reversed from surplus to deficit. In Stage 3, with the increase of sulfate aerosol concentration and its mixing with dust, aerosols showed strong scattering characteristics. Observations showed that DSR decreased by 744 $W \cdot m^{-2}$ from 12:30 to 17:00 on March 25. The decrease rate was 8% higher than that under clear-sky background (the same period in Stage 1-2). This further reflects that the radiative properties of different types of aerosols can change the surface-atmosphere radiation balance and heating or cooling rate, and then change the PBL structure. The strong scattering effect of sulfate aerosols combined with water vapor accumulation provided the necessary thermodynamic preconditions for the subsequent condensation and outbreak of sea fog in the near-surface layer.

The corresponding paragraph in the conclusions section has been revised to:

The cold-air intrusion and dust radiative forcing co-acted to change the boundary-layer thermodynamic structure, constructing a favourable background for the formation of advection sea fog. During Stage 2, the solar diurnal cycle together with the co-acting effects of cold-air advection and dust jointly modulated the attenuation of DSR at the surface. This caused the near-surface temperature to drop sharply by 5.0°C within 5 hours, forming an inversion. The inversion was mainly concentrated at 0.4-1 km, with the maximum inversion intensity reaching 9°C. Previous studies on advection sea fog mostly emphasized the advective cooling effect. However, this study found that under a high-dust background, dust radiative effects combined with synoptic-scale cold-air advection to deepen the inversion during the early stage of Stage 2. This process enhanced the stability of the boundary layer in advance. This early inversion (Stage 2) superimposed with the subsequently established warm and moist advection (the SAT-SST was 1.8°C in Stage 3), providing favourable thermodynamic conditions and stratification stability for the occurrence of sea fog. During the advection sea fog period (Stage 4), the dense fog layer caused the net radiation (Rn) to remain continuously negative. This kept the MEE at a high level of 70-120 m^2/g, establishing the long-term maintenance of the sea fog system. The study found that DLR was the most sensitive to the state changes of sea fog (fluctuations of fog top height, uneven liquid water content, and fog layer thickness).